Statistics of overpressure fluctuations behind a weak shock wave interacting with turbulence

Kento Inokuma, Tomoaki Watanabe ⬥, Koji Nagata ⬥, and Yasuhiko Sakai ⬥

View Online   Export Citation   CrossMark

Statistics of overpressure fluctuations behind a weak shock wave interacting with turbulence

Kento Inokuma,[1] Tomoaki Watanabe,[1,a)] Koji Nagata,[1] and Yasuhiko Sakai[2]

AFFILIATIONS

[1] Department of Aerospace Engineering, Nagoya University, Nagoya 464-8603, Japan
[2] Department of Mechanical Systems Engineering, Nagoya University, Nagoya 464-8603, Japan

[a)]watanabe.tomoaki@c.nagoya-u.jp

ABSTRACT

The overpressure fluctuations behind a weak shock wave interacting with turbulence are studied by wind tunnel experiments, where a spherical shock wave propagates in grid turbulence. The experiments are conducted for various values of the shock Mach number M_{S0} of the shock wave and turbulent Mach number M_T of the grid turbulence. The experimental results show that the root-mean-squared peak-overpressure fluctuation divided by the averaged peak-overpressure, $\sigma_{\Delta p}/\langle \Delta p \rangle$, where the inherent noise caused by the experimental facility is removed, follows a power law of $M_T^2/(M_{S0}^2 - 1)$. The probability density functions of the overpressure fluctuations are close to the Gaussian profile for a wide range of $M_T^2/(M_{S0}^2 - 1)$. A shock deformation model based on the deformation due to nonuniform fluid velocity is proposed for the investigation of the influences of turbulence on the shock wave. The deformation changes the cross-sectional area of the ray tube, which is related to the shock Mach number fluctuation of the area. The model for a weak shock wave yields the relation $\sigma_{\Delta p}/\langle \Delta p \rangle \approx (1/\sqrt{3})[M_T^2/(M_{S0}^2 - 1)]^{1/2}$, which agrees well with the experimental results. The model also predicts the Gaussianity of the peak-overpressure fluctuations behind the shock wave interacting with Gaussian velocity fluctuations. Good agreements between the model and experiments imply that the change in the shock wave characteristics by the interaction with turbulence is closely related to the shock wave deformation caused by the fluctuating turbulent velocity field.

Published under license by AIP Publishing. https://doi.org/10.1063/1.5110185

I. INTRODUCTION

Shock waves can be found in a wide range of physics problems, such as star formation by supernova explosion[1] and inertial confinement fusion.[2] They are also important in engineering applications, where high speed flows in a propulsion system and those around supersonic aircraft generate shock waves.[3,4] In such problems, the shock waves propagate in a fluid, whose motion is described by the Navier–Stokes equations. The fluid motion can easily become turbulent because of the nonlinearity of the governing equations, and in this case, the shock waves propagate in turbulence, which is characterized by complex fluid motions with a wide range of spatial and temporal scales.

The shock wave propagation in turbulence causes the shock/turbulence interaction,[5] which changes both characteristics of the shock wave and turbulence. This has often been experimentally and numerically studied in shock/turbulent boundary layer

interaction problems.[6–10] The interaction induces the fluctuations of the shock wave strength, defined in terms of the shock Mach number or jump in the pressure or density across the shock wave. Since the shock Mach number is one of the important parameters in the flow with shock waves, the prediction and modeling of turbulence effects on the shock wave strength have been considered as important subjects in shock wave research. Therefore, the characteristics of the shock wave propagating in turbulence have been studied in previous studies.

Numerical simulations have found that the shock wave propagation in turbulence can result in the shock holes, which are locally broken regions of the shock wave, across which jumps in physical quantities do not exist.[11–13] Numerical studies[11–14] and a theoretical study[15] have been attempted to find parameters that characterize the influence of turbulence on the shock wave. These previous studies have considered the shock Mach number $M_{S0} = U_{S0}/a_0$, turbulent Mach number $M_T = \sqrt{2k_T}/a_0$, and turbulent Reynolds

number $Re_\lambda = u_{rms}\lambda/\nu$ as dominant parameters in the turbulence effects on the shock wave, where a_0 is the speed of sound in front of the shock wave, U_{S0} is the propagation speed of the shock wave, k_T is the turbulent kinetic energy, u_{rms} is the root-mean-squared (rms) velocity fluctuation, λ is the Taylor microscale, and ν is the kinematic viscosity. For example, previous numerical studies have proposed various criteria under which the shock holes appear. It is suggested that the shock holes appear when $M_T^2/(M_{S0} - 1) \gtrsim$ 0.1 in Lee *et al.*,[11] $M_T^2/(M_{S0}^2 - 1) \gtrsim 0.06$ in Larsson and Lele,[12] and $M_T/(M_{S0} - 1) \gtrsim 0.6$ in Larsson *et al.*[13] The nondimensional parameters $M_T/(M_{S0} - 1)$ and $M_T^2/(M_{S0}^2 - 1)$, considered as the measure of the relative strength of turbulence to the shock wave, are often used to understand the interaction between turbulence and the shock wave.[11–15] However, so far, there is no consensus on nondimensional parameters that characterize the turbulence effects on the shock wave. Donzis[15] theoretically indicated that the variance of the fluctuation in the dilatation of the shock wave normalized by the mean dilatation increases with $M_T/(M_{S0} - 1)$. The dilatation fluctuation was estimated from the ratio of the velocity jump across the shock wave and shock thickness fluctuation in the analysis, where the fluctuations of the velocity jump are ignored. However, the fluctuations of the pressure jump, which are closely related to the fluctuations of the velocity jump by the Rankine-Hugoniot relations, were confirmed in previous studies.[11,13,14,16–18] Both experiments and numerical simulations have shown that the turbulent velocity fluctuation in the shock normal direction has correlation with the fluctuation of the overpressure behind the shock wave at a low turbulent Mach number.[14,18] It is therefore important to experimentally and theoretically examine the relation between these parameters and the jump in physical variables across the shock wave.

In the present study, experiments are conducted for the interaction between a weak spherical shock wave and grid turbulence. A spherical shock wave is one of the canonical shock waves, and it has been extensively studied by theories, experiments, and numerical simulations.[19–24] A weak shock wave is expected to be suitable for the investigation of the parameters $M_T/(M_{S0} - 1)$ and $M_T^2/(M_{S0}^2 - 1)$ since the difference between these two parameters becomes large for such a shock wave with $M_{S0} \approx 1$. The interaction between a weak shock wave and turbulence is also important in various problems. For example, the shock wave in the sonic boom problem is weak at the ground level, and the measured overpressure is of order of 10^1–10^2 Pa.[25] Predictions of the sonic boom caused by the shock wave during the supersonic flight need models for the influences of the atmospheric turbulence on the shock wave.[26] The purpose of this study is to experimentally and theoretically assess the nondimensional parameters that characterize the effects of turbulent velocity fluctuations on the shock wave characteristics.

In this paper, we propose a shock deformation model for the investigation of the turbulence effects on the shock wave. The shock deformation model was used in our previous studies for the explanation of the response time of the overpressure modulation of the shock wave by turbulence, which was observed both in experiments[18] and numerical simulations.[14] The model considers the shock wave deformation caused by a nonuniform velocity profile. The model is extended to investigate the shock Mach number fluctuation caused by the deformation: following the approximate

theory by Whitham,[27] in our model, we obtain the local shock Mach number fluctuation from the change in the ray tube area associated with the deformation. Our model is compared with the experimental results of the statistics of the overpressure fluctuation behind the shock wave.

II. EXPERIMENTS OF SPHERICAL SHOCK WAVE PROPAGATING IN GRID TURBULENCE

A. Experimental methods

Experiments are conducted for the interaction between a spherical shock wave and grid turbulence in a wind tunnel for various values of M_T and M_{S0} so that we can cover a wide range of $M_T/(M_{S0} - 1)$ and $M_T^2/(M_{S0}^2 - 1)$. Here, our experiments are restricted to grid turbulence at a low turbulent Mach number (incompressible turbulence) to prevent fluctuations of thermodynamic properties from affecting the shock wave. Because grid turbulence is a good approximation of homogeneous isotropic turbulence, we can also eliminate the influence of mean velocity gradients, which exists in the shock wave propagating in free shear flows.[28]

Figure 1(a) shows the side view of the experimental setup. The wind tunnel and the shock generator used in this study are the same as those in our previous studies.[17,18,29] A square grid with a mesh size of M (a solidity of 0.36) is installed at the entrance to the test section. Grid turbulence with the mean streamwise velocity of U_0 develops behind the grid. The properties of the grid turbulence in the present wind tunnel are reported in Kitamura *et al.*[30] On the other hand, the shock wave is produced with the shock generator based on a quick piston valve, by which the driver gas (air of 900 kPa) is released into the driven gas (air of ambient pressure). After the shock wave is ejected from the open end of the shock tube, it spherically spreads and propagates in the grid turbulence. A pressure transducer (PCB Piezotronics, Inc., 113B27) mounted on the horizontal plate[18] is used for the overpressure measurements. The rise time of the pressure transducer is less than 1 μs. The resolution of the pressure measurements by our pressure transducer
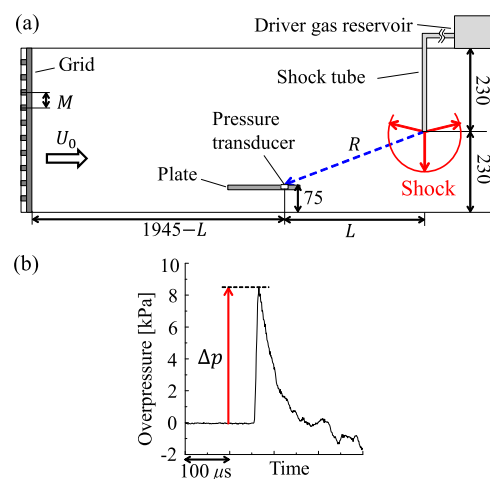

FIG. 1. (a) Experimental setup. Lengths are shown in mm. (b) Example of the time history of the overpressure for case 1.

is 0.007 kPa. Pressure transducers with similar performance have been used for the overpressure measurements in the experiments on shock/turbulence interactions (e.g. Refs. 17 and 28). Sasoh *et al.* used the same experimental facility as ours, and measured the overpressure with the pressure transducer with the same resolution as ours.[17] In their study, the overpressure fluctuations caused by turbulence were well resolved for the investigations of the turbulence effects on the histogram of overpressure fluctuations, averaged overpressure, and rms overpressure fluctuations.[17] The pressure signals are sampled at a frequency of 1 MHz with an oscilloscope (YOKOGAWA, DL850E), where the sampling is started before the shock wave is ejected.

The experiments are conducted for eight conditions shown in Table I, which are considered by changing M, U_0, and the streamwise location of the pressure measurements, which is shown as the streamwise distance L from the open-end of the shock tube to the pressure measurement location. For each case, 400 runs of the shock wave ejections are conducted to take ensemble average, which is denoted by $\langle\rangle$. Figure 1(b) shows an example of the time history of the overpressure for case 1 with the definition of the peak-overpressure Δp observed upon the arrival of the shock wave. The overpressure sharply rises by the arrival of the shock wave and gradually decays with time because of an expansion wave that follows the shock wave. This waveform is typical for a spherical shock wave and similar to those obtained in previous studies.[16,23,24,28,31] The shock Mach numbers M_{S0} shown in Table I are estimated from the ensemble averages of Δp, $\langle\Delta p\rangle$. Streamwise velocity measurements by hot wire anemometry (DANTEC DYNAMICS, Streamline) with an I-type hot wire probe (DANTEC DYNAMICS, 55P11) are conducted in grid turbulence. Statistics of the streamwise velocity are computed with time average $\overline{*}$. Table I summarizes the characteristics of the grid turbulence at the same streamwise location as the pressure transducer. Figure 2 shows the streamwise velocity variance $u_{rms}^2 = \overline{U^2} - \overline{U}^2$ divided by $\overline{U}^2$ for $M = 100$ (mm) at $U_0 = 10$ or 20 (m/s) as a function of the streamwise distance from the grid, x_1. $(u_{rms}/\overline{U})^2$ decays with a power law. Least square method yields the power laws as $(u_{rms}/\overline{U})^2 = 0.059(x_1/M - 2.5)^{-1.1}$ for $U_0 = 10$ (m/s) and $(u_{rms}/\overline{U})^2 = 0.071(x_1/M - 2.2)^{-1.1}$ for $U_0 = 20$ (m/s), where virtual origins x_0/M are 2.5 and 2.2, respectively. The decay exponents agree with previous experiments[30] for a similar range of x_1/M. The turbulent Mach number is defined with $M_T = \sqrt{3}u_{rms}/a_0$ in isotropic turbulence. The same definition is also used for the
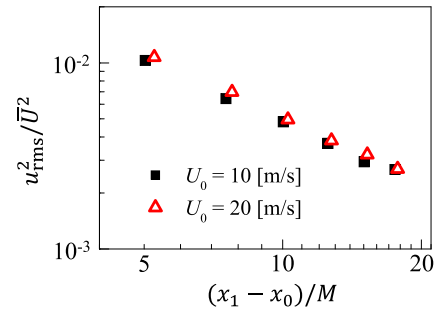

FIG. 2. $(u_{rms}/\overline{U})^2$ plotted against $(x_1 - x_0)/M$ for $M = 100$ (mm) at $U_0 = 10$ and 20 (m/s).

grid turbulence in this paper because the rms values of streamwise and transverse velocity fluctuations are close to each other.[30] In the present experiments, M_T changes depending on M, U_0, and L while the shock Mach number M_{S0} at the pressure measurement location depends on L because of the decay of M_{S0} with the propagation of the spherical shock wave.

B. Averaged peak-overpressure

Figure 3 plots $\langle\Delta p\rangle$ against the distance between the open end of the shock tube and pressure measurement location, $R = \sqrt{L^2 + 155^2}$ (mm). According to Landau,[19] $\langle\Delta p\rangle$ of a spherical shock wave decays with R as $\langle\Delta p\rangle \propto 1/(R\sqrt{\ln(R/k_1)})$, where k_1 is a constant. The least square method applied to $\langle\Delta p\rangle$ in the present study yields $\langle\Delta p\rangle = 830/(R\sqrt{\ln(R/179)})$ (kPa). The changes in $\langle\Delta p\rangle$ in cases with same R are less than 2% despite that they have different turbulence conditions, confirming that the difference in M_T considered in our experiments does not have large effects on $\langle\Delta p\rangle$.

C. Peak-overpressure fluctuations

Statistical analyses are conducted for the fluctuation of Δp defined as $\Delta p' = \Delta p - \langle\Delta p\rangle$. Figure 4 shows the probability density functions (pdfs) of $\Delta p'$ normalized by $\Delta p'_{rms} = \langle\Delta p'^2\rangle^{1/2}$. The Gaussian profile is also shown in Fig. 4, which seems to be in good agreement with the experimental results. To quantitatively evaluate the
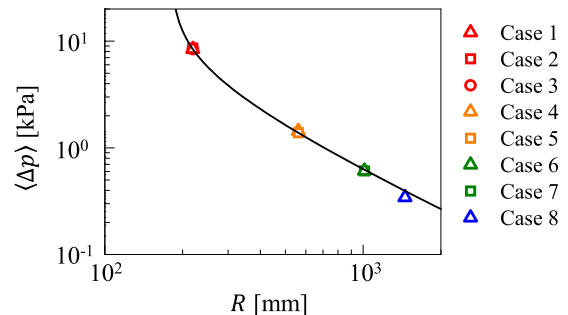
TABLE I. Experimental conditions. $Re_M = U_0 M/\nu$ is the grid Reynolds number. u_{rms}, M_T, and M_{S0} are values at the pressure measurement location [1945 $- L$ (mm) behind the grid].

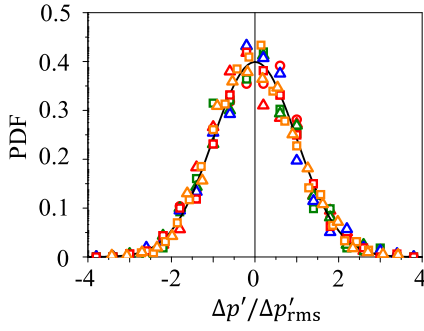| Case	1	2	3	4	5	6	7	8
M (mm)	15	50	100	50	100	100	100	100
U_0 (m/s)	10	10	10	10	10	10	20	20
$Re_M \times 10^{-4}$	0.98	3.3	6.5	3.4	6.7	6.5	13	13
L (mm)	155	155	155	540	540	1000	1000	1445
u_{rms} (m/s)	0.141	0.316	0.545	0.377	0.636	0.850	1.76	3.20
$M_T \times 10^4$	7.12	15.9	27.4	19.0	32.0	42.8	88.7	161
M_{S0}	1.021	1.021	1.021	1.004	1.004	1.002	1.002	1.001

FIG. 3. $\langle\Delta p\rangle$ of each case plotted against R. The solid line shows $\langle\Delta p\rangle = 830/(R\sqrt{\ln(R/179)})$ (kPa).

FIG. 4. Pdfs of $\Delta p'/\Delta p'_{\rm rms}$ of each case. Symbols are common to Fig. 3. Black solid line shows the Gaussian profile.

Gausianity of the pdfs in Fig. 4, we calculate the skewness and flatness of $\Delta p'$. Figure 5 shows the skewness $\langle \Delta p'^3\rangle/\Delta p'^3_{\rm rms}$ and flatness $\langle \Delta p'^4\rangle/\Delta p'^4_{\rm rms}$ against $M_{\rm T}^2/(M_{\rm S0}^2-1)$. It is confirmed that the skewness and flatness of $\Delta p'$ range from 0 to 0.4 and from 2.8 to 3.5, respectively, which are close to the values of the Gaussian profile (0 for skewness and 3 for flatness). Thus, the pdf of $\Delta p'$ is close to the Gaussian profile for $O(10^{-6}) \le M_{\rm T}^2/(M_{\rm S0}^2-1) \le O(10^{-2})$. Numerical simulations[11–13] have investigated the density jump $\Delta\rho$ across the shock wave, where a linear relation can be found between $\Delta p'$ and the density jump fluctuation $\Delta\rho'$ as $\Delta p'/\langle\Delta p\rangle = m\Delta\rho'/\langle\Delta\rho\rangle$ [Eq. (A5)]. In numerical simulations by Larsson et al.,[13] the pdfs of $\Delta\rho$ are slightly skewed at higher $M_{\rm T}$ for $O(10^{-2}) \le M_{\rm T}^2/(M_{\rm S0}^2-1) \le O(10^{-1})$. However, the skewness of $\Delta\rho$ at $M_{\rm T}^2/(M_{\rm S0}^2-1) = 0.018$ and 0.11 estimated from their pdfs of $\Delta\rho$ are about 0.44 and 0.65, respectively, which are also not far from the Gaussian value.

In experiments of shock waves, there exist the peak-overpressure fluctuations that are inherently caused by an experimental facility. In our study, these can be evaluated by the experiments of the shock wave ejected in the flow without the grid, where the rms value of $\Delta p'$ is denoted by $(\Delta p'_{\rm w/o})_{\rm rms}$. Following previous study,[17] the peak-overpressure fluctuations caused by turbulence are evaluated as $\sigma_{\Delta p} = [\Delta p'^2_{\rm rms} - (\Delta p'_{\rm w/o})^2_{\rm rms}]^{1/2}$.

Figures 6(a) and 6(b) show $\sigma_{\Delta p}/\langle\Delta p\rangle$ plotted against $M_{\rm T}/(M_{\rm S0}-1)$ and $M_{\rm T}^2/(M_{\rm S0}^2-1)$, respectively. The figures include the results of the previous experiments and numerical simulations
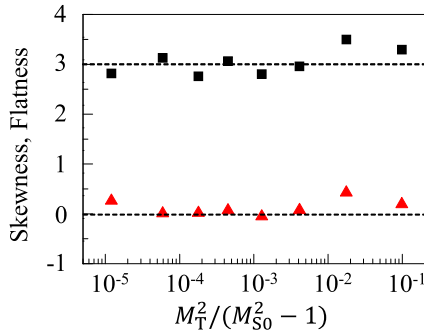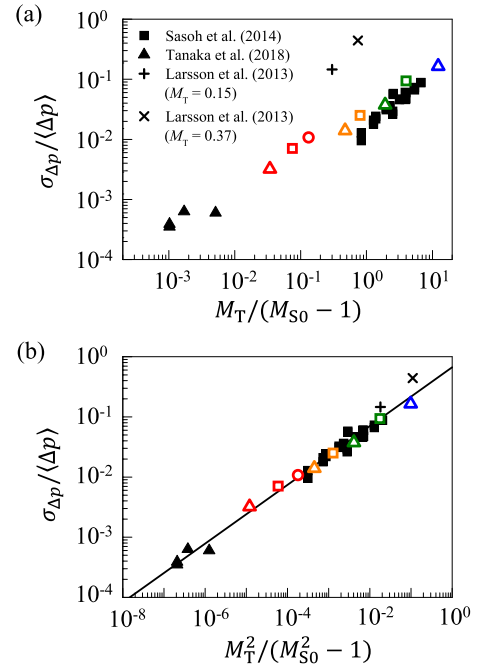

FIG. 6. $\sigma_{\Delta p}/\langle\Delta p\rangle$ plotted against (a) $M_{\rm T}/(M_{\rm S0}-1)$ and (b) $M_{\rm T}^2/(M_{\rm S0}^2-1)$. Symbols are common to Fig. 3. $\sigma_{\Delta p}/\langle\Delta p\rangle$ obtained by Sasoh et al.[17] and Tanaka et al.[14] are also plotted in the figures. $\sigma_{\Delta p}/\langle\Delta p\rangle$ estimated from the results by Larsson et al.[13] are also shown for comparison. The straight line in (b) shows the power law $\sigma_{\Delta p}/\langle\Delta p\rangle = 0.669[M_{\rm T}^2/(M_{\rm S0}^2-1)]^{0.489}$ obtained by using the least squared method for $\sigma_{\Delta p}/\langle\Delta p\rangle$.

of the interaction between a shock wave and grid turbulence or homogeneous isotropic turbulence. Here, the experiments of the interaction between the spherical shock wave and grid turbulence were conducted by Sasoh et al.[17] for $M_{\rm S0} = 1.0009$ and low $M_{\rm T} = O(10^{-4}–10^{-3})$. Numerical simulations of a planar shock wave propagating in homogeneous isotropic turbulence by Tanaka et al.[14] were conducted for a low turbulent Mach number $M_{\rm T} = O(10^{-4})$ and $M_{\rm S0} = 1.1, 1.3$, and 1.5. The figures also include $\sigma_{\Delta p}/\langle\Delta p\rangle$ obtained with Eq. (A6) in the numerical simulations of a planar shock wave at $M_{\rm S0} = 1.5$ interacting with compressible turbulence at high turbulent Mach numbers ($M_{\rm T} = 0.15$ or 0.37) by Larsson et al.[13] Here, the rms fluctuation of $\Delta\rho$ divided by its mean value $\langle\Delta\rho\rangle$, $\sigma_{\Delta\rho}/\langle\Delta\rho\rangle$, is estimated from the pdfs of $\Delta\rho$ shown in their paper. For fixed $M_{\rm S0}$ ($M_{\rm S0} = 1.0009$ in Sasoh et al.[17] and $M_{\rm S0} = 1.002, 1.004$, and 1.021 in the present study), $\sigma_{\Delta p}/\langle\Delta p\rangle$ tends to increase with $M_{\rm T}$. However, the results with different $M_{\rm S0}$ follow a different line in Fig. 6(a). On the other hand, $\sigma_{\Delta p}/\langle\Delta p\rangle$ plotted against $M_{\rm T}^2/(M_{\rm S0}^2-1)$ tends to collapse onto a single line in the logarithmic plot in Fig. 6(b), where $\sigma_{\Delta p}/\langle\Delta p\rangle$ obeys a power law of $M_{\rm T}^2/(M_{\rm S0}^2-1)$. The spherical shock waves used in Fig. 6 have different curvature radii R depending on the experiments. In the present experiments, R ranges between 219 mm and 1453 mm while $R = 215$ (mm) is constant in Sasoh et al.[17] Some of the experiments in the present study and in Sasoh et al. are conducted for similar values of $M_{\rm T}^2/(M_{\rm S0}^2-1)$ but with different R. Comparison among these experiments shows that the relation between $\sigma_{\Delta p}/\langle\Delta p\rangle$ and $M_{\rm T}^2/(M_{\rm S0}^2-1)$ is not affected by R.

FIG. 5. Skewness (triangle) and flatness (square) of $\Delta p'$ as a function of $M_{\rm T}^2/(M_{\rm S0}^2-1)$.

The least square method applied to the data points in Fig. 6(b) yields $\sigma_{\Delta p}/\langle \Delta p \rangle = 0.669[M_T^2/(M_{S0}^2 - 1)]^{0.489}$ as shown in Fig. 6(b).

III. SHOCK DEFORMATION MODEL OF TURBULENCE EFFECTS ON SHOCK WAVE

A. Shock wave deformation by nonuniform velocity profile

We study the overpressure fluctuations behind a shock wave interacting with turbulence with a shock deformation model, which considers a planar shock wave deformed by a local velocity fluctuation. In this model, we explain the effects of turbulence on a shock wave as the shock wave deformation due to nonuniformity of the velocity field. The model assumes that the velocity gradient in the shock tangential direction plays an important role in the shock deformation. The importance of the velocity gradient in the tangential direction was also confirmed in our recent numerical simulations, where strong correlation between the pressure gradient across the shock wave and the velocity gradient of turbulence was reported.[14] Therefore, the effects of turbulence are studied with the simplified model with the velocity profile that is nonuniform only in the shock tangential direction. The model is used to estimate the overpressure fluctuation level induced by the deformation.

The velocity fluctuation in the model is given by an axisymmetric velocity profile $u_M(x, r)$, where x and r are the axial and radial coordinates. Temporal evolution of velocity fluctuations is not taken into account because of the small velocity fluctuation $u_{rms} \ll U_{S0}$ in the present experiments, where the time scale of the turbulence is much larger than that of the shock wave propagation. A simple profile of u_M is considered in the model,

$$u_M(x, r) = \begin{cases} u & (0 \le r \le r_0 \text{ and } 0 \le x \le x_l) \\ 0 & \text{otherwise} \end{cases}, \quad (1)$$

which has a constant velocity u in the cylindrical region defined with r_0 and x_l. The model considers influences of turbulence, where a large part of turbulent kinetic energy is contained in large-scale turbulent motions. Therefore, the distribution of u_M is related to large-scale motions. Thus, both r_0 and x_l are comparable with an integral length scale, where anisotropy of large scales is assumed to be weak as in the case of grid turbulence.

The model considers the planar shock wave propagating into the velocity field $u_M(x, r)$ in the x direction as illustrated in Fig. 7(a). The velocity of the shock wave movement is given by the sum of the shock propagation velocity $U_{S0} = a_0 M_{S0}$ and the fluid velocity on the shock wave. The shock movement velocity is U_{S0} for $r > r_0$ and $U_{S0} + u$ for $r \le r_0$. Therefore, once the planar shock wave begins to propagate in the region with the velocity fluctuation u, the velocity of the shock wave movement becomes nonuniform and the shock wave begins to be deformed. However, since the shock wave surface needs to be connected at $r = r_0$, the inclination of the surface occurs from $r = r_0$. Therefore, the shock ray at $r = r_0$ also begins to be inclined as shown in Fig. 7(a), where the trajectories of the shock rays passing through $(x, r) = (0, r_0)$ are also shown with blue lines. The region surrounded by the infinite number of these shock rays is called a ray tube. The cross-sectional area A of the ray tube changes from $A = \pi r_0^2$ at $x = 0$ as the shock wave propagates. Once the trajectory of the shock ray (x_R, r_R) is determined,
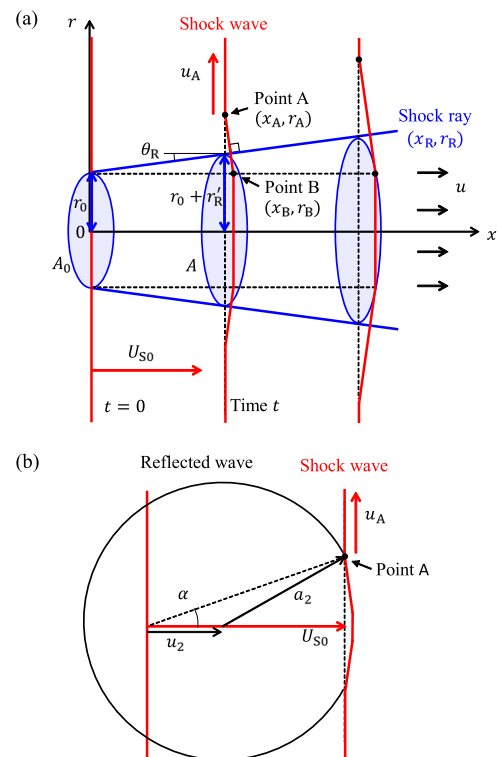

FIG. 7. (a) Shock wave deformation due to a local velocity fluctuation u and (b) reflected wave propagation on the shock wave surface.

A at given $x = x_R$ can be computed as $A = \pi r_R^2$. The change in the area A results in the change in the shock Mach number M_S of the area.[27] The present model considers the turbulence effects on the shock Mach number through the change in A due to the velocity fluctuation u_M.

In the following discussion, the trajectories of the shock rays are obtained from the geometry of the shock wave because the shock ray is locally perpendicular to the shock wave surface. The change in M_S causes the pressure change behind the shock wave in the region of $r \le r_0$. Then, a spherical reflected wave is formed because of the pressure change as shown in Fig. 7(b). For simplicity, the reflected wave is assumed to be isentropic, and the propagation of the reflected wave in the region of $r \le r_0$ is not discussed below. The intersection of the nondeformed part of the shock wave and the reflected wave is shown as point A in Fig. 7(b). The reflected wave propagates with the characteristic velocity represented as the sum of the fluid velocity and sound speed behind the shock wave.[32] Figure 7(b) shows the schematic of the reflected wave propagation on the shock wave surface, where a_2 and u_2 are the sound speed and fluid velocity behind the shock wave in the laboratory coordinate system, respectively. Here, u_2 and a_2 are assumed to be constant and independent from the change in M_S because $M_S' \equiv M_S - M_{S0} \ll M_{S0}$. The propagation velocity of the reflected wave in the r direction on the shock wave surface, u_A, is obtained from the geometrical relation of a_2, U_{S0}, and u_2,

$$u_A = \sqrt{a_2^2 - (U_{S0} - u_2)^2}, \tag{2}$$

which is also constant. The initial position of point A is $(x_A, r_A) = (0, r_0)$. Therefore, the trajectory of point A (x_A, r_A) is given by

$$x_A(t) = U_{S0}t, \tag{3}$$

$$r_A(t) = u_A t + r_0. \tag{4}$$

According to the Rankine-Hugoniot relations,

$$u_2 = \frac{2a_0}{\gamma + 1}\left(M_{S0} - \frac{1}{M_{S0}}\right) \tag{5}$$

and

$$a_2 = a_0 \frac{\sqrt{(2\gamma M_{S0}^2 - \gamma + 1)\{(\gamma - 1)M_{S0}^2 + 2\}}}{(\gamma + 1)M_{S0}}. \tag{6}$$

In Fig. 7(b), α denotes the angle between the trajectory of point A and x axis in the laboratory coordinate system. From Eqs. (2), (5), and (6), $\tan\alpha = u_A/U_{S0}$ is written as a function of M_{S0},

$$\tan\alpha = \frac{1}{M_{S0}^2}\sqrt{\frac{\{(\gamma - 1)M_{S0}^2 + 2\}(M_{S0}^2 - 1)}{\gamma + 1}}. \tag{7}$$

As the shock wave propagates, point A also propagates in r direction at speed u_A, and the inclined region of the shock wave expands. The phenomenon of the expansion of the inclined region caused by the reflected wave was also confirmed by previous experimental study on shock wave reflections over wedges[33] and theoretical study on shock-vortex interactions.[34] In the present model, the shock wave surface in $r_0 \leq r \leq r_A$ is described by the line connecting points A and B in Fig. 7(a). The trajectory of point B is obtained from $(dx_B/dt, dr_B/dt) = (U_{S0} + a_0 M_S' + u, 0)$, where the change in the Mach number due to the interaction with the velocity fluctuation is taken into account as $a_0 M_S'$,

$$x_B(t) = (U_{S0} + u)t + a_0 \int_0^t M_S'(t^*)dt^*, \tag{8}$$

$$r_B(t) = r_0. \tag{9}$$

Because the shock ray is perpendicular to the line AB, the trajectory of the shock ray (x_R, r_R) can be determined as

$$\tan\theta_R \equiv \frac{dr_R}{dx_R} = \frac{x_B - x_A}{r_A - r_B}. \tag{10}$$

Substituting Eqs. (3), (4), (8), and (9) into Eq. (10) yields

$$\tan\theta_R = \frac{ut + a_0 \int_0^t M_S'(t^*)dt^*}{u_A t}. \tag{11}$$

With the trapezoidal rule, the integration in the numerator in Eq. (11) can simply be estimated as $\int_0^t M_S'(t^*)dt^* \approx M_S't/2$ with the initial condition $M_S' = 0$ at $t = 0$,

$$\tan\theta_R \approx \frac{u + a_0 M_S'/2}{u_A}. \tag{12}$$

For the ray tube whose radius is r_0 at $x_R = 0$, its radius r_R at any time t can be calculated with Eq. (12). Then, the radius deviation $r_R' = r_R - r_0$ is

$$r_R' = \int_0^{x_R} \tan\theta_R dx_R^* \approx \int_0^{x_R} \frac{u + a_0 M_S'/2}{u_A}dx_R^*. \tag{13}$$

The deviation of $A = \pi r_R^2$ from $A_0 = \pi r_0^2$, $A' = A - A_0$ can be written as

$$A' \approx 2\pi r_0 r_R' \approx 2\pi r_0 \int_0^{x_R} \frac{u + a_0 M_S'/2}{u_A}dx_R^*, \tag{14}$$

where we consider small deformation $A' \ll A_0$ in the model. Equation (14) gives the fluctuation of the ray tube area as a function of $x_R(t)$, which increases with time as the shock wave propagates. A'/A_0 can be written as

$$\frac{A'}{A_0} \approx \frac{2\pi r_0 r_R'}{\pi r_0^2} \approx 2\int_0^{x_R} \frac{u + a_0 M_S'/2}{U_{S0}\tan\alpha} \frac{dx_R^*}{r_0} \equiv 2\xi. \tag{15}$$

B. Shock Mach number fluctuation for a weak shock wave

Hereafter, a weak shock wave is considered in the model as the present experiments are conducted for weak shock waves. The analysis for a strong shock wave is presented in Appendix B. The shock Mach number M_S of the ray tube with the area A is obtained from the relation[27]

$$\frac{A}{A_0} = \exp\left(-\int_{M_{S0}}^{M_S} g(M_S^*)dM_S^*\right), \tag{16}$$

where M_S^* is an integration variable. Here,

$$g(M_S) \equiv \frac{M_S}{M_S^2 - 1}\left(2\mu + 1 + \frac{1}{M_S^2}\right)\left(1 + \frac{2}{\gamma + 1}\frac{1 - \mu^2}{\mu}\right) \tag{17}$$

and

$$\mu^2 \equiv \frac{(\gamma - 1)M_S^2 + 2}{2\gamma M_S^2 - \gamma + 1}, \tag{18}$$

where γ is the heat capacity ratio. For a weak shock wave ($M_{S0} \to 1$), Eq. (16) can be simplified[35] as

$$\frac{A}{A_0} \approx \left(\frac{M_{S0} - 1}{M_S - 1}\right)^2. \tag{19}$$

For $M_{S0} \lesssim 1.1$, Eq. (19) can calculate the $A-M_S$ relation of Eq. (16) with accuracy of more than 90%. From Eqs. (15) and (19), the following relation is obtained for the shock Mach number of the deformed shock wave:

$$\left(\frac{M_{S0} - 1}{M_S - 1}\right)^2 - 1 \approx 2\xi, \tag{20}$$

which can be rewritten as

$$M_S' \approx \frac{(\sqrt{2\xi + 1} - 1)(1 - M_{S0})}{\sqrt{2\xi + 1}} \approx \xi(1 - M_{S0}), \tag{21}$$

where $\sqrt{2\xi + 1} \approx \xi + 1$ is used because $A' \ll A_0$. Differentiating both sides of Eq. (21) with respect to x_R gives the following differential equation:

$$\frac{dM_S'}{dx_R} \approx \frac{1 - M_{S0}}{r_0}\frac{u + a_0 M_S'/2}{U_{S0}\tan\alpha}. \tag{22}$$

The solution of Eq. (22) is

$$M_S' \approx -\frac{2u}{a_0}\left[1 - \exp\left(-\frac{M_{S0}-1}{2M_{S0}\tan\alpha}\frac{x_R}{r_0}\right)\right], \quad (23)$$

which yields M_S' as a function of x_R. Since the model assumes $x_l/r_0 \approx 1$, $M_{Sl}' \equiv M_S'(x_l)$ is written as

$$M_{Sl}' \approx -\frac{2u}{a_0}\left[1 - \exp\left(-\frac{M_{S0}-1}{2M_{S0}\tan\alpha}\right)\right]. \quad (24)$$

For $M_{S0} \to 1$, $\exp\left(-\frac{M_{S0}-1}{2M_{S0}\tan\alpha}\right) \approx 1 - \frac{M_{S0}-1}{2M_{S0}\tan\alpha}$, and Eq. (24) can be simplified as

$$M_{Sl}' \approx -\frac{u}{a_0}\frac{M_{S0}-1}{M_{S0}\tan\alpha}. \quad (25)$$

According to the Rankine-Hugoniot relations, Δp at $x_R = x_l$ is

$$\Delta p = \frac{2\gamma p_0}{\gamma+1}\left[(M_{S0}+M_{Sl}')^2 - 1\right], \quad (26)$$

where p_0 is the mean pressure in front of the shock wave. The ensemble average of Eq. (26) is

$$\langle\Delta p\rangle = \frac{2\gamma p_0}{\gamma+1}(M_{S0}^2 + \langle M_{Sl}'^2\rangle - 1), \quad (27)$$

where $M_{S0} = \langle M_S\rangle$. For $M_{Sl}' \ll M_{S0}$, Eq. (27) gives

$$\langle\Delta p\rangle \approx \frac{2\gamma p_0}{\gamma+1}(M_{S0}^2 - 1). \quad (28)$$

On the other hand, the overpressure fluctuation $\Delta p' = \Delta p - \langle\Delta p\rangle$ is

$$\Delta p' = \frac{2\gamma p_0}{\gamma+1}(2M_{S0}M_{Sl}' + M_{Sl}'^2 - \langle M_{Sl}'^2\rangle). \quad (29)$$

The terms of the second order of M_{Sl}' can be ignored in Eq. (29). Therefore, the following expression can be obtained:

$$\Delta p' \approx \frac{4\gamma}{\gamma+1}p_0 M_{S0}M_{Sl}'. \quad (30)$$

Equations (25), (28), and (30) yield the following relation between $\Delta p'$ and the velocity fluctuation:

$$\frac{\Delta p'}{\langle\Delta p\rangle} \approx \frac{2M_{S0}}{M_{S0}^2-1}M_{Sl}' \approx -\frac{u/a_0}{\tan\alpha}, \quad (31)$$

where $M_{S0} + 1 \approx 2$ for $M_{S0} \to 1$ is used. Here, $\tan\alpha$ given by Eq. (7) is simply represented as a function of the initial shock Mach number M_{S0}.

When the pdf of u follows the Gaussian profile as in many canonical turbulent flows,[36] the linear relation between $\Delta p'$ and u in Eq. (31) shows that the pdf of $\Delta p'$ also follows the Gaussian profile. This explains the Gaussian pdf of the peak-overpressure fluctuations observed in Fig. 4 because grid turbulence has Gaussian velocity fluctuations. The standard deviations of both sides of Eq. (31) yield the relation among the rms peak-overpressure fluctuation, mean peak overpressure, shock Mach number, and turbulent Mach number,

$$\frac{\sigma_{\Delta p}}{\langle\Delta p\rangle} \approx \frac{1}{\sqrt{3}}\left(\frac{M_T^2}{M_{S0}^2-1}\right)^{1/2}, \quad (32)$$

where $\tan\alpha \approx \sqrt{M_{S0}^2-1}$ is used because the weak shock wave has $M_{S0} \to 1$. Hence, $\sigma_{\Delta p}/\langle\Delta p\rangle$ can be represented as a simple function of $M_T^2/(M_{S0}^2-1)$. This relation is well supported by the experimental results of the weak shock waves shown in Fig. 6(b), where the fitting to the power law $\sigma_{\Delta p}/\langle\Delta p\rangle = a[M_T^2/(M_{S0}^2-1)]^b$ yields $a = 0.669$ and $b = 0.489$, both of which agree well with Eq. (32). Thus, the present model obtains Eq. (32) from the deformation of the shock wave and the relation between the ray tube area and shock Mach number. Previous studies[11,12] also reported that $M_T^2/(M_{S0}^2-1)$ is an important parameter in the fluctuations of the shock wave dilatation or broken shock wave conditions. This parameter was considered as the ratio of the turbulent pressure fluctuations $\rho_0 u_{rms}^2$ (ρ_0 is the density in front of a shock wave) to Δp. The present model also implies that the shock Mach number fluctuation caused by the shock wave deformation is also important in the broken shock wave and the dilatation fluctuation.

C. Inclination angle of a shock wave

In classical studies, Ribner constructed a model for the shock inclination caused by a periodic velocity perturbation.[37,38] In this section, we compare the shock inclination angle obtained in our model with that obtained in Ribner's model. From Eqs. (12) and (25), we have the inclination angle of our model,

$$\frac{\tan\theta_R}{u/a_0} \approx \frac{1}{M_{S0}\tan\alpha}\left[1 - \frac{M_{S0}-1}{2M_{S0}\tan\alpha}\right]. \quad (33)$$

On the other hand, Ribner assumed the shock inclination angle to be a sinusoidal function,[37] whose amplitude and wave number were determined by the sinusoidal velocity perturbation given in front of the shock wave, relation of the velocity across the shock wave, and linear perturbation theory. We let θ_R obtained in his study be θ_{RA}. θ_{RA} can be written as $\theta_{RA} = \theta_{RA0}\sin ky$, where θ_{RA0} is the amplitude, k is the wave number, and y is the coordinate in the shock tangential direction. $\tan\theta_{RA0}$ can be written as

$$\frac{\tan\theta_{RA0}}{u/a_0} \approx \frac{1}{M_{S0}}\frac{4\sqrt{1-\left(\frac{U_{S0}-u_2}{a_2}\right)^2}\frac{U_{S0}}{U_{S0}-u_2}}{(\gamma+1)\left(\frac{U_{S0}}{U_{S0}-u_2}-1\right)}$$

$$= 2M_{S0}\sqrt{\frac{\gamma+1}{(2\gamma M_{S0}^2-\gamma+1)(M_{S0}^2-1)}}, \quad (34)$$

where $U_{S0} - u_2$ is the velocity behind the shock wave in the shock fixed coordinate system, and $\theta_{RA0} \approx \tan\theta_{RA0}$ is used because of $\theta_{RA0} \ll 1$. In Fig. 8, we compare Eq. (33) with Eq. (34). While both are decrease functions of M_{S0}, Eq. (34) is almost twice as large as Eq. (33) in $M_{S0} \leq 1.5$. This is because $\tan\theta_R/(u/a_0) \to 1/\sqrt{M_{S0}^2-1}$ when $M_{S0} \to 1$ while $\tan\theta_{RA0}/(u/a_0) \to 2/\sqrt{M_{S0}^2-1}$ when $M_{S0} \to 1$. It is interesting that in both approaches, the inclination angle can be proportional to u/a_0 and $1/\sqrt{M_{S0}^2-1}$ for $M_{S0} \to 1$. With Eq. (34), however, A' becomes twice as large as that obtained with Eq. (14), resulting in twice the value of $\sigma_{\Delta p}/\langle\Delta p\rangle$ than that obtained with Eq. (32) because of the linear relation among θ_R, A' and $\Delta p'$ described by Eqs. (15), (21), and (30).
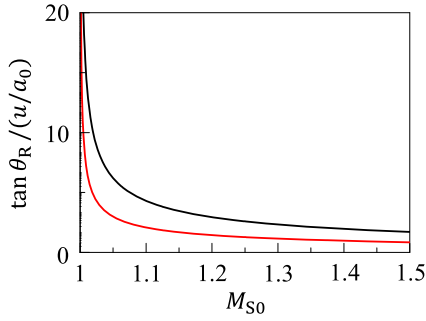
FIG. 8. $\tan\theta_R/(u/a_0)$ plotted against M_{S0}. Red and black lines are $\tan\theta_R/(u/a_0)$ obtained with Eq. (33) and $\tan\theta_{RA0}/(u/a_0)$ obtained with Eq. (34), respectively.

D. Condition for broken shock wave

The broken region of the shock wave surface is considered in the shock deformation model for the weak shock wave. The broken shock wave does not have a distinct jump in physical quantities at some parts of the shock wave surface, and the overpressure Δp in the broken region is much smaller than the average value $\langle\Delta p\rangle$. Here, the present paper uses the term "broken region" to represent a local region without the jump on the shock wave surface while "broken shock wave" denotes the shock wave where the broken regions occupy an important fraction of the area on the shock wave surface. The broken region is detected as $\Delta\rho \leq \alpha_{\rho B}\langle\Delta\rho\rangle$. $\alpha_{\rho B}$ is chosen based on the results of numerical simulations of interactions between a planar shock wave and turbulence by Larsson et al.,[13] where the statistics of the density jump, $\Delta\rho$, across the shock wave were studied in detail. Because of Eq. (A5), $\Delta\rho \leq \alpha_{\rho B}\langle\Delta\rho\rangle$ is equivalent to $\Delta p \leq \alpha_{pB}\langle\Delta p\rangle$, where $\alpha_{pB} \equiv m(\alpha_{\rho B} - 1) + 1$. Their simulations with $M_T = 0.37$ and $M_{S0} = 1.5$, which is considered as the broken shock wave case, show that the broken region is well detected by $\alpha_{\rho B}$ between 0.1 and 0.6 (α_{pB} between 0.017 and 0.56). For $\alpha_{\rho B} = 0.1$ and 0.6 ($\alpha_{pB} = 0.017$ and 0.56), the detected broken regions occupy 0.05% and 10% on the shock wave surface, respectively.

A cumulative distribution function of $\Delta p/\langle\Delta p\rangle$, $F(\alpha)$, that represents a probability of events with $\Delta p/\langle\Delta p\rangle \leq \alpha$ can be obtained by integrating the pdf of $\Delta p/\langle\Delta p\rangle$ from 0 to α. Since the broken region is defined as $\Delta p/\langle\Delta p\rangle \geq \alpha_{pB}$, $F(\alpha = \alpha_{pB})$ yields the fraction of the broken regions on the shock wave surface. F can be computed from the pdf of $\Delta p'/\langle\Delta p\rangle$. The pdf of u is assumed to follow the Gaussian profile as in grid turbulence,

$$\text{PDF}(u) = \frac{1}{\sqrt{2\pi}}\exp\left(-\frac{u^2}{2u_{\text{rms}}^2}\right). \quad (35)$$

In this case, the pdf of $\Delta p'/\langle\Delta p\rangle$ in the shock deformation model is also expressed by the Gaussian profile because of the linear relation between u and $\Delta p'$ in Eq. (31). The pdf of $\Delta p'/\langle\Delta p\rangle$ is obtained as a function of $M_T^2/(M_{S0}^2 - 1)$ because the variance of $\Delta p'/\langle\Delta p\rangle$ is written as Eq. (32). Therefore, $F(\alpha)$ in the shock deformation model depends on the parameter $M_T^2/(M_{S0}^2 - 1)$. The fraction of the broken regions $F(\alpha_{pB}; M_T^2/(M_{S0}^2 - 1))$ is numerically computed for $\alpha_{pB} = 0.017$ and 0.56 in $10^{-2} \leq M_T^2/(M_{S0}^2 - 1) \leq 10^0$. Figure 9 shows F as a function of $M_T^2/(M_{S0}^2 - 1)$. When $M_T^2/(M_{S0}^2 - 1)$ is of order of 10^{-1}, the fraction of the broken regions for $0.017 \leq \alpha_{pB} \leq 0.56$
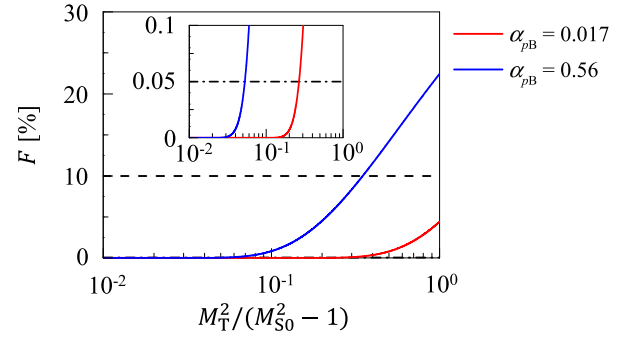

FIG. 9. Cumulative distribution function $F(\alpha_{pB})$, which represents the probability of $\Delta p/\langle\Delta p\rangle \leq \alpha_{pB}$ for $\alpha_{pB} = 0.017$ (red) and 0.56 (blue), plotted against $M_T^2/(M_{S0}^2 - 1)$. Horizontal dashed-dotted line and broken line show $F = 0.05$ (%) and 10 (%), respectively.

rapidly increases, and F for $\alpha_{pB} = 0.017$ and $\alpha_{pB} = 0.56$ exceed 0.05% and 10%, respectively. Therefore, the broken shock wave is expected to appear for $M_T^2/(M_{S0}^2 - 1) \geq O(10^{-1})$. This condition is consistent with the numerical results,[11–13] where the broken shock wave was also found for $M_T^2/(M_{S0}^2 - 1) \geq O(10^{-1})$. It is important to note that these numerical simulations consider compressible turbulence at much higher turbulent Mach number than in the present experiments. The model does not consider temperature and density fluctuations, which can exist in front of the shock wave propagating through compressible turbulence. Therefore, the model might not be accurate for the shock/turbulence interaction with high turbulent Mach number.

Compressible turbulence at high turbulent Mach number causes fluctuations in density and temperature as well as fluid properties such as a viscosity coefficient, and the influences of compressible turbulence on the shock wave are much more complicated than those of incompressible turbulence. It should be noted that in Fig. 6(b), $\sigma_{\Delta\rho}/\langle\Delta\rho\rangle$ at $M_T = 0.37$ by Larsson et al.[13] shows a greater deviation from the fitting line than at $M_T = 0.15$, indicating that the compressibility of turbulence can affect the fluctuations in the density or pressure jump across a shock wave. Therefore, in the case with compressible turbulence, the broken shock wave can be caused even at smaller $M_T^2/(M_{S0}^2 - 1)$ than in the case with incompressible turbulence though in both cases, the broken shock criterion can be $M_T^2/(M_{S0}^2 - 1) \geq O(10^{-1})$.

IV. CONCLUDING REMARKS

We have conducted wind tunnel experiments on a weak spherical shock wave propagating in grid turbulence at a low turbulent Mach number and have investigated the statistics of peak-overpressure fluctuations for various values of $M_T^2/(M_{S0}^2 - 1)$. The rms peak-overpressure fluctuation normalized by the averaged peak-overpressure, $\sigma_{\Delta p}/\langle\Delta p\rangle$, is shown to follow a power law of $M_T^2/(M_{S0}^2 - 1)$. Fitting of experimental results in present and previous studies indicates $\sigma_{\Delta p}/\langle\Delta p\rangle = 0.669[M_T^2/(M_{S0}^2 - 1)]^{0.489}$. The pdfs of the peak-overpressure fluctuations are very close to the Gaussian profile for a wide range of $M_T^2/(M_{S0}^2 - 1)$ from $O(10^{-6})$ to $O(10^{-2})$.

We have proposed the shock deformation model for the influences of turbulence on the shock wave. The model relates the shock

Mach number fluctuation induced by turbulence to the shock wave deformation due to the nonuniform velocity fluctuation, where the change in the cross-sectional area of the ray tube caused by the deformation produces the shock Mach number fluctuation. The model for a weak shock wave yields the relation $\sigma_{\Delta p}/\langle \Delta p \rangle \approx (1/\sqrt{3})[M_{\mathrm{T}}^2/(M_{\mathrm{S}0}^2 - 1)]^{1/2}$, which is consistent with the experimental results. The Gaussianity of the peak-overpressure fluctuations is also obtained from the model when the velocity fluctuations are Gaussian, which is also consistent with the present experiments. The model also predicts that the broken shock wave appears in the case of $M_{\mathrm{T}}^2/(M_{\mathrm{S}0}^2 - 1) \geq O(10^{-1})$.

ACKNOWLEDGMENTS

APPENDIX A: RELATION BETWEEN Δp AND $\Delta \rho$

The sound speed equation behind the shock wave is

$$a_2^2 = \frac{\gamma(\langle \Delta p \rangle + p_0)}{\langle \Delta \rho \rangle + \rho_0}. \tag{A1}$$

From the isentropic relation,[11]

$$\Delta p' = a_2^2 \Delta \rho'. \tag{A2}$$

From Eqs. (A1) and (A2) and the sound speed equation in front of the shock wave $a_0^2 = \gamma p_0/\rho_0$, the relation between $\Delta p'/\langle \Delta p \rangle$ and $\Delta \rho'/\langle \Delta p \rangle$ is obtained as follows:

$$\frac{\Delta p'}{\langle \Delta p \rangle} = \frac{\gamma \Delta \rho'}{\langle \Delta \rho \rangle + \rho_0 - \frac{\gamma p_0}{a_2^2}} = \frac{\gamma \Delta \rho'}{\langle \Delta \rho \rangle + \rho_0\left(1 - \frac{a_0^2}{a_2^2}\right)}. \tag{A3}$$

According to the Rankine-Hugoniot relations,

$$\frac{\langle \Delta \rho \rangle}{\rho_0} = \frac{2(M_{\mathrm{S}0}^2 - 1)}{(\gamma - 1)M_{\mathrm{S}0}^2 + 2}. \tag{A4}$$

From Eqs. (6), (A3), and (A4), we have

$$\frac{\Delta p'}{\langle \Delta p \rangle} = \frac{2\gamma M_{\mathrm{S}0}^2 - \gamma + 1}{(\gamma + 1)M_{\mathrm{S}0}^2}\frac{\Delta \rho'}{\langle \Delta \rho \rangle} = m\frac{\Delta \rho'}{\langle \Delta \rho \rangle}, \tag{A5}$$

where $m \equiv (2\gamma M_{\mathrm{S}0}^2 - \gamma + 1)/\{(\gamma + 1)M_{\mathrm{S}0}^2\}$. The standard deviation of Eq. (A5) yields

$$\frac{\sigma_{\Delta p}}{\langle \Delta p \rangle} = m\frac{\sigma_{\Delta \rho}}{\langle \Delta \rho \rangle}. \tag{A6}$$

APPENDIX B: SHOCK MACH NUMBER FLUCTUATION FOR A STRONG SHOCK WAVE

For a strong shock wave ($M_{\mathrm{S}0} \to \infty$), Eq. (16) can be simplified[35] as

$$\frac{A}{A_0} \approx \left(\frac{M_{\mathrm{S}0}}{M_{\mathrm{S}}}\right)^n, \tag{B1}$$

where $n = \lim_{M_{\mathrm{S}} \to \infty}\{(M_{\mathrm{S}}^2 - 1)g/M_{\mathrm{S}}\} \approx 5.0743$. For $M_{\mathrm{S}0} \gtrsim 2.6$, Eq. (B1) assures accuracy of more than 90% for the $A - M_{\mathrm{S}}$ relation of Eq. (16). From Eqs. (15) and (B1), M_{S}' is written as

$$M_{\mathrm{S}}' \approx \frac{1 - (2\xi + 1)^{1/n}}{(2\xi + 1)^{1/n}}M_{\mathrm{S}0} \approx -\frac{2}{n}\xi M_{\mathrm{S}0}, \tag{B2}$$

where $(2\xi + 1)^{1/n} \approx 2\xi/n + 1$ ($\xi \ll 1$) is used for small deformation. Differentiation of both sides of Eq. (B2) with respect to x_{R} yields

$$\frac{\mathrm{d}M_{\mathrm{S}}'}{\mathrm{d}x_{\mathrm{R}}} \approx -\frac{2M_{\mathrm{S}0}}{n}\frac{u + a_0 M_{\mathrm{S}}'/2}{U_{\mathrm{S}0}\tan\alpha}\frac{1}{r_0}. \tag{B3}$$

The solution of Eq. (B3) is

$$M_{\mathrm{S}}' \approx -\frac{2u}{a_0}\left[1 - \exp\left(-\frac{1}{n\tan\alpha}\frac{x_{\mathrm{R}}}{r_0}\right)\right]. \tag{B4}$$

Therefore, $M_{\mathrm{S}l}' \equiv M_{\mathrm{S}}'(x_l)$ is

$$M_{\mathrm{S}l}' \approx -\frac{2u}{a_0}\left[1 - \exp\left(-\frac{1}{n\tan\alpha}\right)\right] = -c\frac{u}{a_0}, \tag{B5}$$

where $x_l/r_0 \approx 1$ is used and c is defined as $c \equiv 2\left[1 - \exp\left(-\frac{1}{n\tan\alpha}\right)\right]$. From Eqs. (28), (30), and (B5), $\Delta p'/\langle \Delta p \rangle$ for $M_{\mathrm{S}0} \to \infty$ is written as

$$\frac{\Delta p'}{\langle \Delta p \rangle} \approx -\frac{2M_{\mathrm{S}0}}{M_{\mathrm{S}0}^2 - 1}c\frac{u}{a_0} \approx -2c\frac{u/a_0}{M_{\mathrm{S}0}}, \tag{B6}$$

Since $c \approx 0.7658$ for $M_{\mathrm{S}0} \to \infty$, we have

$$\frac{\Delta p'}{\langle \Delta p \rangle} \approx -1.532\frac{u/a_0}{M_{\mathrm{S}0}}. \tag{B7}$$

The standard deviations of Eq. (B7) yield the following relation among $\sigma_{\Delta p}/\langle \Delta p \rangle$, $M_{\mathrm{S}0}$, and M_{T}:

$$\frac{\sigma_{\Delta p}}{\langle \Delta p \rangle} \sim \frac{M_{\mathrm{T}}}{M_{\mathrm{S}0}}. \tag{B8}$$

REFERENCES

[1]M.-M. Mac Low and R. S. Klessen, "Control of star formation by supersonic turbulence," Rev. Mod. Phys. **76**, 125 (2004).

[2]V. A. Thomas and R. J. Kares, "Drive asymmetry and the origin of turbulence in an ICF implosion," Phys. Rev. Lett. **109**, 075004 (2012).

[3]C. B. Pepper, M. A. Nascarella, and R. J. Kendall, "A review of the effects of aircraft noise on wildlife and humans, current control mechanisms, and the need for further study," Environ. Manage. **32**, 418–432 (2003).

[4]D. J. Maglieri, "Some effects of airplane operations and the atmosphere on sonic-boom signatures," J. Acoust. Soc. Am. **39**, S36–S42 (1966).

[5]Y. Andreopoulos, J. H. Agui, and G. Briassulis, "Shock wave-turbulence interactions," Annu. Rev. Fluid Mech. **32**, 309–345 (2000).

[6]L. Agostini, L. Larchevêque, and P. Dupont, "Mechanism of shock unsteadiness in separated shock/boundary-layer interactions," Phys. Fluids **27**, 126103 (2015).

[7]H. Ozawa, "Experimental study of unsteady aerothermodynamic phenomena on shock-tube wall using fast-response temperature-sensitive paints," Phys. Fluids **28**, 046103 (2016).

[8]N. Li, J. Chang, K. Xu, D. Yu, W. Bao, and Y. Song, "Prediction dynamic model of shock train with complex background waves," Phys. Fluids **29**, 116103 (2017).

[9]X. Fang, C. Shen, M. Sun, and Z. Hu, "Effects of oblique shock waves on turbulent structures and statistics of supersonic mixing layers," Phys. Fluids **30**, 116101 (2018).

[10] Y. Zhuang, H. Tan, X. Li, F. Sheng, and Y. Zhang, "Görtler-like vortices in an impinging shock wave/turbulent boundary layer interaction flow," Phys. Fluids **30**, 061702 (2018).

[11] S. Lee, S. K. Lele, and P. Moin, "Direct numerical simulation of isotropic turbulence interacting with a weak shock wave," J. Fluid Mech. **251**, 533–562 (1993).

[12] J. Larsson and S. K. Lele, "Direct numerical simulation of canonical shock/turbulence interaction," Phys. Fluids **21**, 126101 (2009).

[13] J. Larsson, I. Bermejo-Moreno, and S. K. Lele, "Reynolds- and Mach-number effects in canonical shock-turbulence interaction," J. Fluid Mech. **717**, 293–321 (2013).

[14] K. Tanaka, T. Watanabe, K. Nagata, A. Sasoh, Y. Sakai, and T. Hayase, "Amplification and attenuation of shock wave strength caused by homogeneous isotropic turbulence," Phys. Fluids **30**, 035105 (2018).

[15] D. A. Donzis, "Shock structure in shock-turbulence interactions," Phys. Fluids **24**, 126101 (2012).

[16] B. Lipkens and D. T. Blackstock, "Model experiment to study sonic boom propagation through turbulence. Part II. Effect of turbulence intensity and propagation distance through turbulence," J. Acoust. Soc. Am. **104**, 1301–1309 (1998).

[17] A. Sasoh, T. Harasaki, T. Kitamura, D. Takagi, S. Ito, A. Matsuda, K. Nagata, and Y. Sakai, "Statistical behavior of post-shock overpressure past grid turbulence," Shock Waves **24**, 489–500 (2014).

[18] K. Inokuma, T. Watanabe, K. Nagata, A. Sasoh, and Y. Sakai, "Finite response time of shock wave modulation by turbulence," Phys. Fluids **29**, 051701 (2017).

[19] L. D. Landau, "On shock waves at large distances from the place of their origin," J. Phys. USSR **9**, 496–500 (1945).

[20] R. F. Chisnell, "The motion of a shock wave in a channel, with applications to cylindrical and spherical shock waves," J. Fluid Mech. **2**, 286–298 (1957).

[21] G. B. Whitham, "On the propagation of shock waves through regions of non-uniform area or flow," J. Fluid Mech. **4**, 337–360 (1958).

[22] F. G. Friedlander, "The diffraction of sound pulses I. Diffraction by a semi-infinite plane," Proc. R. Soc. London, Ser. A **186**, 322–344 (1946).

[23] C. E. Needham, *Blast Waves* (Springer, 2010).

[24] S. M. Liang, J. S. Wang, and H. Chen, "Numerical study of spherical blast-wave propagation and reflection," Shock Waves **12**, 59–68 (2002).

[25] H. W. Carlson, "Experimental and analytical research on sonic boom generation at NASA," NASA SP 147, 1967, p. 9.

[26] A. D. Pierce, "Statistical theory of atmospheric turbulence effects on sonic-boom rise times," J. Acoust. Soc. Am. **49**, 906–924 (1971).

[27] G. B. Whitham, "A new approach to problems of shock dynamics. Part 1. Two-dimensional problems," J. Fluid Mech. **2**, 145–171 (1957).

[28] J. H. Kim, A. Sasoh, and A. Matsuda, "Modulations of a weak shock wave through a turbulent slit jet," Shock Waves **20**, 339–345 (2010).

[29] T. Kitamura, K. Nagata, Y. Sakai, A. Sasoh, and Y. Ito, "Changes in divergence-free grid turbulence interacting with a weak spherical shock wave," Phys. Fluids **29**, 065114 (2017).

[30] T. Kitamura, K. Nagata, Y. Sakai, A. Sasoh, O. Terashima, H. Saito, and T. Harasaki, "On invariants in grid turbulence at moderate Reynolds numbers," J. Fluid Mech. **738**, 378–406 (2014).

[31] E. Salze, P. Yuldashev, S. Ollivier, V. Khokhlova, and P. Blanc-Benon, "Laboratory-scale experiment to study nonlinear N-wave distortion by thermal turbulence," J. Acoust. Soc. Am. **136**, 556–566 (2014).

[32] F. Grasso and S. Pirozzoli, "Shock-wave–vortex interactions: Shock and vortex deformations, and sound production," Theor. Comput. Fluid Dyn. **13**, 421–456 (2000).

[33] A. Sasoh, K. Takayama, and T. Saito, "A weak shock wave reflection over wedges," Shock Waves **2**, 277–281 (1992).

[34] P. Clavin, "Nonlinear analysis of shock–vortex interaction: Mach stem formation," J. Fluid Mech. **721**, 324–339 (2013).

[35] G. B. Whitham, "A new approach to problems of shock dynamics. Part 2. Three-dimensional problems," J. Fluid Mech. **5**, 369–386 (1959).

[36] S. B. Pope, *Turbulent Flows* (IOP Publishing, 2001).

[37] H. S. Ribner, "Convection of a pattern of vorticity through a shock wave," NACA Report No. 1164, 1954.

[38] H. S. Ribner, "Shock-turbulence interaction and the generation of noise," NACA Report No. 1233, 1955.